Scattering of Polarized Laser Light by Water Droplet, Mixed-Phase and Ice Crystal Clouds. Part II: Angular Depolarizing and Multiple-Scattering Behavior

KENNETH SASSEN AND KUO-NAN LIOU

Department of Meteorology, University of Utah, Salt Lake City 84112

(Manuscript received 17 October 1978, in final form 15 January 1979)

ABSTRACT

Light scattering measurements obtained with a polar nephelometer in the planes of polarization both orthogonal and parallel to that of the linearly polarized laser source are used to investigate the angular depolarizing properties of artificial ice, water and mixed-phase clouds in Part II of this report. Although the generation of depolarized energy in water and ice clouds is shown to be accomplished by different scattering mechanisms, angular depolarization patterns for both cloud types display the tendency for linear depolarization ratios (δ, the ratio of orthogonal to parallel polarized signals) to increase with increasing scattering angle. For ice clouds, however, the δ values are typically an order of magnitude or more greater than the values for water clouds as a consequence of cloud particle shape effects. Angular depolarization measurements of mixed-phase clouds are shown to possess the potential for determining a measure of cloud ice-water balance by means of bistatic remote sensing observations. Moreover, the backscattering characteristics of water and ice clouds have been examined with the aid of observations performed at a scattering angle of 175° for application to monostatic lidar studies.

1. Introduction

As described in Part I (Sassen and Liou, 1979), significant differences exist in the angular scattering patterns obtained from water and ice clouds as a consequence of the dissimilar cloud particle shapes. From basic scattering theory, pronounced differences from particle shape effects can also be expected at some scattering angles when the depolarization of the incident polarized laser light is considered. These differences in the angular depolarizing properties of water and ice clouds are experimentally examined in Part II. Such information clearly is pertinent to radiation tranfer problems, since the total scattered intensity could be significantly underestimated if the presence of a strong depolarized component is not considered. More importantly, studies of the angular depolarizing behavior of artificial clouds are of fundamental concern to the remote sensing of cloud composition in two respects. First, knowledge of the angular distribution of depolarized energy can contribute to our understanding of the basic single- and multiple-scattering behavior of clouds probed with the backscatter depolarization technique of monostatic lidar. Second, the potential information content of bistatic polarization lidar measurements for cloud composition sensing can be assessed with the aid of such data which cannot at present be adequately predicted through theoretical approaches.

Confining our discussion to particles much larger than the incident wavelength, the depolarization of light energy during scattering results from those multiple internal reflections, or ray paths, which involve the transformation of the scattered electric vibration plane out of the incident plane. For scatterers with spherical symmetry such as cloud droplets, most back- and side-scattering results from external and internal reflections, and surface waves, which produce no depolarization when the scattered light is observed in the planes either parallel or perpendicular to the incident electric vibration plane. Similarly, spherical particle scattering into the forward direction is governed by diffraction and grazing reflections which do not involve any depolarization. However, depolarization can be generated through multiple-scattering activity among members of a concentrated assembly of spheres. The amount of such depolarization measured in the backscatter may become very large after a lidar pulse has penetrated a few hundred meters into a dense water cloud (Pal and Carswell, 1973). As shown by Liou and Schotland (1971), the ratio of primary to second and higher order scattering may decrease rapidly with penetration depth under some conditions of lidar design and cloud content to account for the depolarization increases.

Scattering from nonspherical particles, such as ice crystals, for example, may result in part from non-depolarizing specular (i.e., external) reflections, but

0022-4928/79/050852-10$06.50

strong contributions may be made by multiple internal reflections off the numerous crystal faces. Differences between the angular depolarizing behavior of spherical and nonspherical particles would be most pronounced in the backward and side directions, since forward scattering in both cases is dominated by diffraction. This has been demonstrated through the angular scattering experiments with irregular mineral particles performed by Holland and Gagne (1970), the only previous study to consider the change in polarization properties of the scattered light.

The angular scattering experiments to be reported here for artificial clouds of water and ice particles shed new light on the processes responsible for the depolarization of visible light energy by atmospheric clouds. Special attention is also given to measurements performed as close to the backward scattering direction as possible (i.e., at 175°). The experimental results are shown to have pertinence to both monostatic and bistatic remote sensing techniques for determining cloud composition. Note that the scattering apparatus design and operation have already been described in Part I. Discussed briefly below are the experimental factors of particular concern to the measurement and analysis of the angular depolarization data.

2. Angular depolarization measurements

a. Depolarization data analysis

With the availability of simultaneous records of signals scattered in the planes of polarization orthogonal and parallel to that of the incident vertically or horizontally polarized light, the change in the state of polarization of the scattered light as a function of scattering angle θ can be characterized by the linear depolarization ratio

$$\delta(\theta)=\frac{P_s(\theta)_\perp}{P_s(\theta)_\parallel}, \tag{1}$$

where P_s is the scattered power adjusted for photomultiplier tube gain and the subscripts $\perp$ and $\parallel$ refer to the planes of polarization orthogonal and parallel to that of the source. Note that in terms of the phase matrix elements, the linear depolarization ratios for incident vertically and horizontally polarized light are expressed as $\delta_V=P_{12}/P_{22}$ and $\delta_H=P_{21}/P_{11}$, respectively. The depolarization ratios are calculated from the average signal intensities in each 5° scattering angle interval of recorded data. The data presented here are derived in most cases by averaging the δ values obtained from a number of consecutive scans with the same incident polarization state over a period for which the cloud samples show no significant change in cloud composition. This procedure further reduces the impact of cloud composition fluctuations in the scattering volume. Typical standard deviations

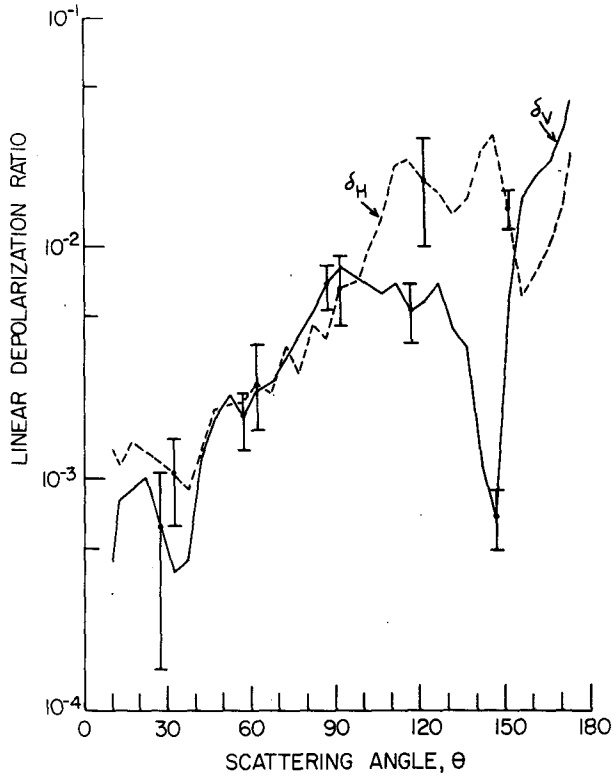

FIG. 1. The dependence of multiple-scattering-induced depolarization in a water cloud on the scattering angle. Data correspond to the phase functions shown on the left side of Fig. 3 in Part I. Average linear depolarization ratios and standard deviations (vertical bars) for incident vertically (δ_V) and horizontally (δ_H) polarized light are shown.

illustrating the variability in δ values are given in the data to follow.

Possible sources of error in the δ values may arise from optical misalignment between the incident polarization plane and receiver prism orientation, and from relative photodetector gain uncertainties. Optical component misalignment of $\leqslant 0.5°$ is ensured by frequent tests, resulting in a maximum error in δ values of <0.01 which may be subtracted from the calculated δ values in an attempt to negate this bias. The relative gains of the two detectors have been independently checked with the use of an unpolarized light source, indicating possible errors on the order of a few percent of the δ values through much of the range of returned signal intensities encountered. It should be noted, however, that δ values derived from one channel displaying the very high signal intensities typical of near-forward scattering may be subject to some additional error from possible photomultiplier tube gain nonlinearities in this region.

b. Water droplet clouds

As demonstrated through the theoretical analysis in Part I, assemblies of spherical particles are pre-

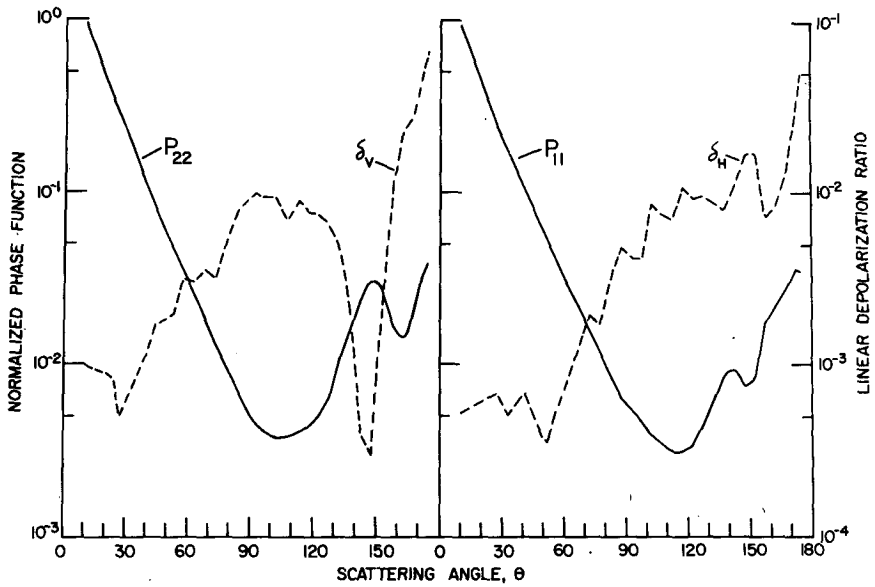

FIG. 2. A comparison of the experimental angular scattering (solid line) and depolarization patterns from single scans of a water cloud with modal drop diameters of 1.5 μm, for incident vertically (left) and horizontally (right) polarized light. Phase functions are normalized with respect to theoretical predictions for an equivalent distribution of spheres at $\theta=10°$.

dicted to generate zero depolarization. This well-known principle provides the basis for discriminating clouds of spherical water drops from nonspherical ice particles, but is rarely realized in scattering measurements of water clouds due to the presence of multiple-scattering activity and experimental errors. In the experimental water cloud data described below, the amounts of depolarization generated through multiple-scattering activity in the optically dense laboratory clouds are appreciably greater than the estimated measurement errors, with the possible exception of the low δ values produced in the near-forward direction.

Shown in Fig. 1 are the averaged angular depolarization patterns for incident vertically (δ_V, solid line) and horizontally (δ_H, dashed line) polarized light which correspond to the parallel-polarized phase functions given on the left side of Fig. 3 of Part I. Typical standard deviations for the averages from the five consecutive water cloud scans are given as vertical bars. In general, it can be seen that δ values are on the order of 0.1% in the near-forward direction, but tend to gradually increase with increasing θ and maximize to values of a few percent at $\theta=175°$. Differences in δ_V and δ_H patterns, however, are particularly evident in the side-to-backscatter region. Interestingly, it is in this same scattering angle interval that the phase functions of Fig. 3 (Part I) also display the greatest differences in values, whereas the values for both the angular scattering and depolarization pattern pairs are roughly equivalent for $\theta\lesssim100°$ and at $\theta=155°$. A comparison of Fig. 1 with Fig. 4 of Part I also demonstrates this feature of the depolarizing behavior of water clouds, where it is evident that the differences in linear depolarization ratios with incident polarization state are generally proportional to the degree of linear polarization.

The relation between the angular scattering and depolarization patterns is further illustrated in Fig. 2, where the patterns from single scans of a different water cloud are given for vertically (left) and horizontally (right) polarized incident light. Although a similar trend of increasing δ values with increasing θ is in evidence, the δ curves (dashed lines) display some dissimilarities induced by the different droplet size distribution in this case. Backscatter δ values, for example, reach 5–6% at $\theta=175°$. As both the scattered intensities and the δ values increase rather strongly in approaching the backscatter, it can be concluded that multiple-scattering activity becomes particularly significant for $\theta>165°$.

c. Ice crystal clouds

Clouds of spherical and nonspherical particles share the scattering mechanisms of diffraction and surface reflection which involve no depolarization of the incident energy. It is in the realm of internal reflections, however, that nonspherical particle scattering becomes distinct, with the generation of depolarized energy representing the signature of this process. Thus, we may expect ice cloud depolarization to be significant in those angular scattering regions where internal reflections contribute importantly.

As illustrated in Fig. 3, the angular depolarizing behavior of ice clouds does indeed depend strongly on the scattering angle, with δ values typically varying

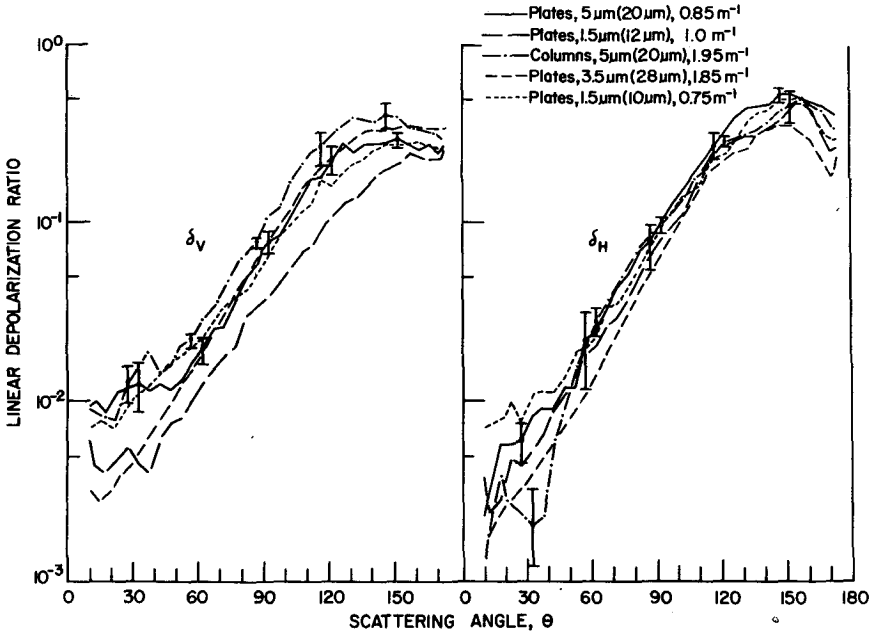

FIG. 3. Angular depolarization patterns for five ice clouds whose compositions are given in the key in terms of dominant ice crystal type, modal crystal maximum dimensions and maximum observed size, and apparent extinction coefficient. Typical standard deviations of the depolarization ratios averaged over several scans are given as vertical bars for two of the experiments, for incident vertically (δ_V) and horizontally (δ_H) polarized light.

by about three orders of magnitude during the nephelometer scan. Shown in the figure are the average depolarization patterns from five ice clouds whose compositions are given in the figure key in terms of dominant ice crystal type, modal maximum dimension and largest observed size, and apparent extinction coefficient. The linear depolarization ratio patterns are given for vertically (δ_V, left) and horizontally

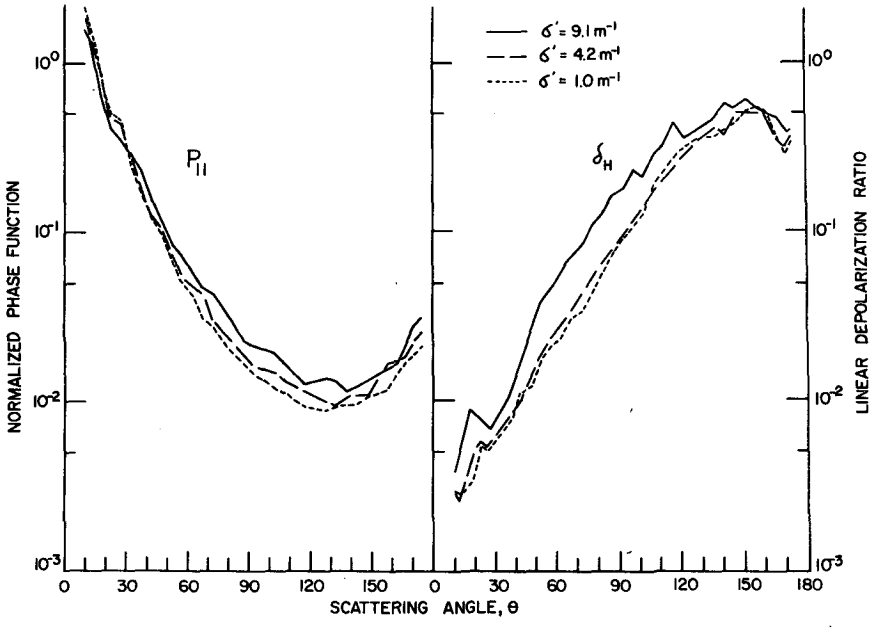

FIG. 4. Experimental angular scattering and depolarization patterns for single scans with incident horizontally polarized light from an ice cloud containing plate crystals (2.5 μm modal maximum dimension). Ice crystal concentrations gradually diminished, as reflected in the change in the extinction coefficients (σ'), during the three scans.

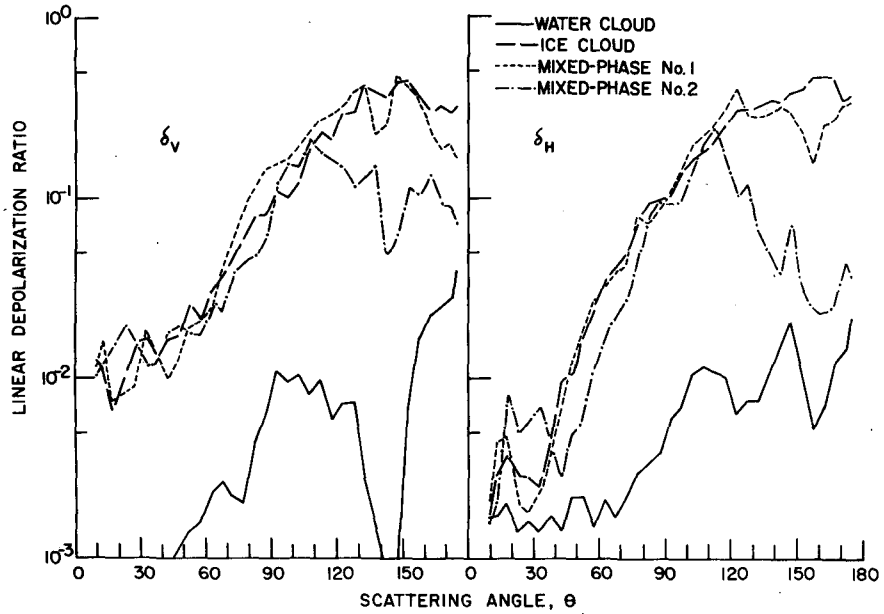

FIG. 5. Angular depolarization patterns from pure water and ice and mixed phase clouds corresponding to the phase functions of Fig. 12 of Part I. Curves labeled Mixed Phase Nos. 1 and 2 represent clouds dominated by ice and water particles, respectively.

(δ_H, right) polarized incident energy. In agreement with our expectations, δ values increase strongly with increasing θ as the contributions from diffraction diminish and those from internal scattering begin to dominate. In the near-forward direction δ values are typically on the order of $\sim 0.5\%$ or less, with the variability in this region perhaps reflecting experimental errors as discussed earlier. For both the δ_V and δ_H patterns the exponential rates of increase in depolarization from about 30–140° are very similar, although the δ_H values are in many cases slightly higher for a given cloud composition in this region. Differences in the generation of depolarization then become apparent as the backscatter is approached. The δ_V values in this region tend to remain constant at a value of ~ 0.3, while the δ_H values reach a maximum value of ~ 0.5 at $\theta \approx 155°$ prior to decreasing to ~ 0.35 by 175°.

It is worthwhile to speculate on the effect of such factors as ice crystal type and size, and ice cloud optical thickness on depolarization. As particularly evident on the left side of Fig. 3, we have often noted the tendency for δ values to increase somewhat in the side-scatter region with increasing crystal thickness and size. The influence of cloud optical thickness on depolarization has also been investigated in an attempt to assess the impact of multiple-scattering activity. The data from single successive scans shown in Fig. 4 were obtained using horizontally polarized incident light from an ice cloud containing simple plate crystals whose concentrations gradually diminished while the size distribution remained relatively constant. Modal crystal dimensions were 2.5 μm, with some particles up to 15 μm. The normalized phase functions [left, from Eq. (14) of Part I] and linear depolarization ratio patterns (right) are given for three stages of the dissipation of the cloud corresponding to extinction coefficients σ' of 9.1, 4.2 and 1.0 m^{-1}. It is evident that the phase functions generally show increased values with increasing σ', particularly in the side-scatter direction. With regard to the degree that the depolarization has been enhanced by the presence of this indicated multiple scattering activity in the clouds, δ values for the $\sigma' = 9.1$ m^{-1} scan are larger by a factor of 2 or more in the side-scatter region than the other two scans which display only small differences from one another. Such observations indicate that there may be a threshold value of ice cloud optical thickness above which depolarization enhancement from multiple-scattering activity becomes significant. The relation between cloud optical thickness and depolarization in the backscatter is examined in a later section with the aid of special observations at $\theta = 175°$.

d. Mixed-phase clouds

The four depolarization patterns given in Fig. 5 for vertically (left) and horizontally (right) polarized incident light correspond to the phase functions for pure water, ice and mixed-phase clouds shown in Fig. 12 of Part I. When the pure water and ice cloud data are compared, it can be seen that while both patterns tend to increase with increasing θ the δ values for ice are typically at least an order of magnitude higher than those generated by multiple scattering in the water cloud. With increasing water content of

the mixed phase clouds (i.e., in going from Mixed Phase No. 1 to No. 2), the transition in the form of angular depolarization pattern from pure ice to water occurs in the following fashion. Initially, δ value decreases are confined primarily to the cloudbow angles due to the strong parallel-polarized contributions from cloud droplets in these regions (see Fig. 12, Part I). These δ value troughs then gradually broaden in angular extent and combine with strong depolarization decreases in approaching true backscattering to give the depolarization patterns a structure which peaks in the side scatter. This characteristic of mixed-phase clouds is due to the fact that the ice-particle-induced depolarization is not greatly influenced by mixed-phase conditions in the side-scatter region where droplets are much less efficient scatterers. In fact, δ values initially increase somewhat in this region in response to an increase in ice crystal size, and begin to decrease only when the droplet population dominates the cloud composition. These features clearly are related to the differences in the relative angular scattering efficiencies of the particles in the two phases.

3. Backscattering measurements and analysis

Scattering observations performed in the backscattering direction have the additional significance of containing information for monostatic remote sensing applications. Some current problem areas of particular concern to the field of lidar meteorology are an inadequate understanding of the multiple-scattering process in water clouds and the lack of knowledge of some scattering parameters for ice crystal clouds. Increased understanding of these factors would enable the differences in water and ice particle scattering behavior to be more fully utilized in the remote determination of cloud composition. Although our backscattering measurements have been performed at a scattering angle of 175°, we believe such data to be helpful in understanding these processes. It should be recognized, however, that measurements performed even 5° from 180° fail to include the effect of the glory for water spheres, while depolarization from ice clouds seems to be somewhat underestimated due to the presence of an apparent trough in δ values at $\theta \approx 175°$.

To examine the effect of cloud droplet multiple scattering on linear depolarization ratios, a number of backscattering measurements have been obtained at $\theta = 175°$ as dense water clouds were alternately permitted to form and dissipate by controlling the input of steam into the chamber. Laser light transmission through the clouds was concurrently monitored, so that the apparent extinction coefficient σ' (see Part I) and cloud optical thickness τ' (σ' times the total cloud path length R) could be derived for comparison to the δ values. Fig. 6 shows the results from a number of such experiments for δ values collected with incident vertically (circles) and horizontally (crosses) polarized light. In agreement with our expectations concerning the causes of depolarization in spherical particles assemblies, δ values can be seen to increase with increasing cloud optical thickness. The rate of depolarization increase with cloud thickness appears to be approximately linear and rather similar for both the δ_H and δ_V values when $\tau' > 0.15$, although δ_V values are on the average ~ 0.01 higher. The scatter in the data points for each incident polarization state is believed to result primarily from changes in the microstructure of the building and dissipating clouds, as the droplet size spectrum has been indicated to have an influence on multiple-scattering-induced depolarization (Liou, 1972). In addition to cloud optical thickness and microstructure, it should be noted that water cloud depolarization measurements are also strongly influenced by the receiver field of view angle, but it has not been possible to study this factor with

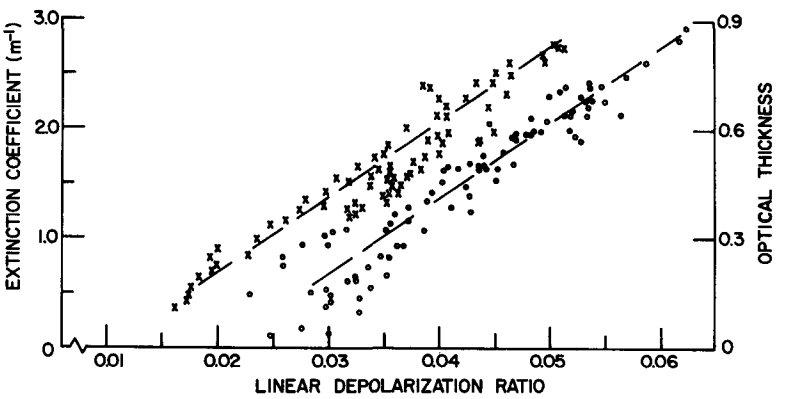

FIG. 6. The dependence of linear depolarization ratios for incident vertically (●) and horizontally (×) polarized light on water cloud optical thickness and extinction coefficient. Dashed lines depict a linear dependence with equivalent slope for the two data sets.

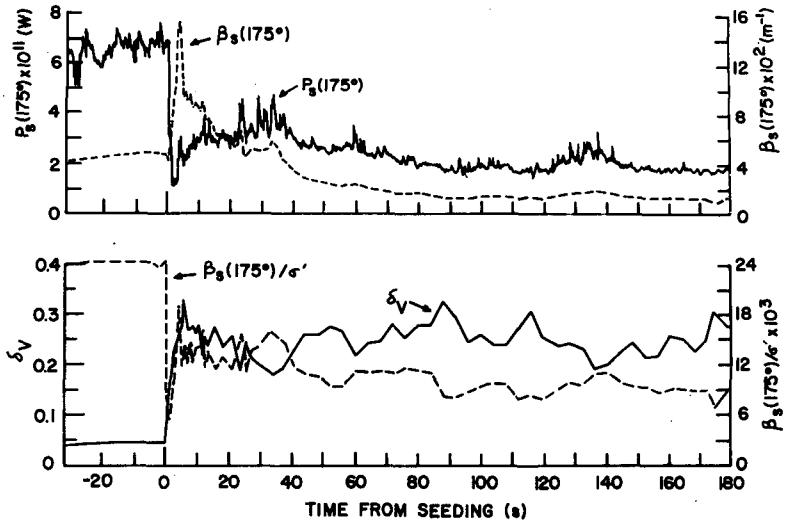

FIG. 7. Variations in various scattering parameters induced by the dry ice seeding of a supercooled water cloud at time $t=0$, as measured at the 175° scattering angle for vertically polarized incident light. The phase transition is accompanied by a decrease in the laser power scattered in the parallel polarization plane (P_S), an increase in the linear depolarization ratio (δ_V) and in the backscattering cross section (β_S), and by oscillations in the approximate backscatter-to-extinction ratio (β_S/σ').

the present receiver design (which views a solid angle of scattered light of 10^{-5} sr).

The influence of optical thickness on ice cloud depolarization at $\theta=175°$ has been studied with the aid of observations performed during massive dry ice seeding which briefly generated extremely dense ice clouds. Shown in Fig. 7 as a function of time from seeding are the variations in $P_S(175°)$ and $\beta_S(175°)$ [top graph, from Eqs. (11) and (13) in Part I] and δ and $\beta_S(175°)/\sigma'$ (bottom graph) which have been induced by the water-to-ice-cloud phase transition. Vertically polarized incident light was used in this experiment. Extinction coefficients increased from 1.95 m^{-1} in the pure water phase to a peak value of 9.6 m^{-1} ($\tau'\approx3.0$) at 1 s after seeding, and then gradually decayed until a value of 1.5 m^{-1} was approached roughly 1.5 min after seeding. A cloud sample initiated with seeding revealed high concentrations of minute plate crystals with a modal diameter of 1.5 μm, and maximum diameters of 6–8 μm. Particle concentrations decreased with time after seeding and the size spectra broadened slightly. In view of the large decrease in σ' values during this period, however, it is likely that the very high extinction coefficients commensurate with the seeding event were caused by the presence of numerous submicron particles which were not collected by the sampling device.

With reference to Fig. 7 it can be seen that the dry ice seeding at time $t=0$ s caused a large drop in P_S values (solid curve, upper graph) but an increase in β_S values (dashed curve) in response to the much higher attenuation. Values of β_S then gradually decrease to below the initial water cloud values with the attainment of stable cloud conditions. Concerning the amount of linear depolarization generated during the phase change, δ values increase rapidly from the 0.04 water cloud value up to 0.33 at 3 s after seeding, clearly illustrating the effect of particle shape on depolarizing properties. Depolarization ratios then fluctuate with time, but can be seen to reach $\sim$0.30 on several occasions despite the changes in the amount of multiple scattering activity associated with variations in τ' through the range of nearly 3.0 to 0.5. The undulations in δ values after seeding can be interpreted in terms of changes in cloud water-ice content if the value of $\delta\approx0.3$ is assumed to represent pure ice phase conditions, as indicated from the previously described angular ice data for $\theta=175°$. That mixed-phase cloud conditions appear to have been present at times following the seeding is also supported by an interpretation of the variations in the $\beta_S(175°)/\sigma'$ parameter discussed below.

Shown as the dashed line in the bottom graph of Fig. 7, the temporal variations in the approximate backscatter-to-extinction ratio, $\beta_S(175°)/\sigma'$, contain additional information regarding the cloud composition. This scattering parameter, which has important remote sensing applications with lidar (see Platt and Bartusek, 1974), is particularly demonstrative of cloud backscattering properties. The effects of scatterer size and concentration on the backscattering coefficient tend to be normalized with the use of this parameter, such that differences in backscattering efficiencies due to particle shape effects become apparent (Sassen, 1978a). It is known from these previous studies that water droplets are more efficient backscatterers than

ice particles and therefore have higher backscatter-to-extinction ratios. This can be readily appreciated from a comparison of the $\beta_S(175°)/\sigma'$ values in Fig. 7 for the water cloud with those obtained after seeding. Interestingly, the experimental values initially decrease sharply after seeding but then reach a peak and undergo further oscillations. This behavior has possibly resulted from the effects of the initial increase in mean ice crystal size for particles which are only slightly larger than the incident wavelength, as illustrated by Platt and Bartusek (1974) for spherical particles. A comparison of the δ and $\beta_S(175°)/\sigma'$ fluctuations after this transitional period in the formation of the ice cloud reveals that the peaks and troughs in the two records are out of phase with respect to one another. This finding supports the conclusion that the depolarization troughs were caused by periods when the more efficient scattering cloud droplets coexisted with the ice crystals.

With the importance of the backscatter-to-extinction ratio for remote sensing applications, the experimentally derived values are given in a different form in Fig. 8 for vertically and horizontally polarized incident light (circles and crosses, respectively). In this figure, the relation between σ' and estimated true backscatter-to-extinction ratio is depicted for water and ice cloud data. The water cloud data, from Fig. 6, have been adjusted for 180° backscattering by multiplying the $\beta_S(175°)/\sigma'$ ratios by factors derived from Mie theory simulations for a number of representative droplet size distributions. These numerical factors, which represent the average theoretical $P(180°)/P(175°)$ ratios, are 1.7 and 1.5 for incident vertical and horizontal light, respectively. Since the relation between cloud backscattering and extinction can be altered by multiple-scattering activity, the backscatter-to-extinction ratio can be expected to increase with optical thickness, as seems to be the case in our data for $\sigma' \gtrsim 1.0$ m^{-1} ($\tau \gtrsim 0.3$). For $\sigma' \lesssim 1.0$ m^{-1}, however, the estimated backscatter-to-extinction ratios do not appear to be greatly sensitive to σ', suggesting that a threshold value of optical thickness may be required in order to induce significant increases in the coefficient ratio. It is also noteworthy that although the average ratio of 0.038 for $\tau' < 0.3$ is smaller than the 0.05 value (divided by 4π) theoretically derived for single scattering by Platt and Bartusek (1974) for cloud droplet size distributions containing somewhat larger drops, the experimental ratio does correspond to the theoretical value for a narrow size distribution with ~ 2 μm modal diameter as supported by the artificial cloud composition data.

As for the data from ice clouds, a similar dependence of the backscatter-to-extinction ratio on σ' can be inferred from Fig. 8. Note that the solid circles represent the data from the seeded cloud of Fig. 7 for points showing $\delta > 0.25$, corresponding to periods when only small amounts of droplets were likely

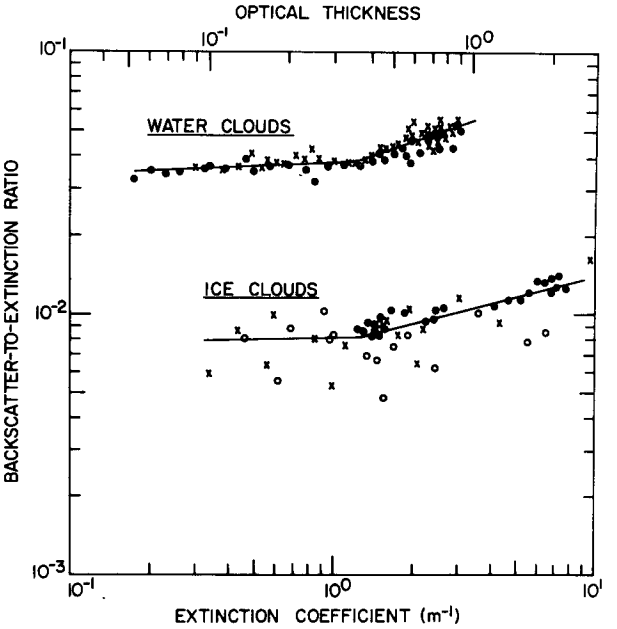

FIG. 8. The variations induced by multiple-scattering activity in the estimated true backscatter-to-extinction ratio as functions of measured extinction and optical thickness. Data are shown for water clouds (from Fig. 6, adjusted for $\theta = 180°$ scattering) and ice clouds (solid circles from Fig. 7), for incident vertically (circles) and horizontally (crosses) polarized light.

present. The remaining data points were gathered from a number of nephelometer scans at $\theta = 175°$ for both incident polarization states and comprise a range of ice crystal types and sizes which have likely contributed to the scatter in the data. Since clouds of nonspherical particles would lack the glory intensity maxima, it has been assumed that $\beta_S(175°) \approx \beta_S(180°)$ for the experimental ice cloud data. In comparison to the characteristic backscatter-to-extinction ratio of 0.05 for "large" water spheres, the ice cloud values for $\sigma' < 1.0$ m^{-1} can be seen to range between factors of 5 and 10 smaller.

4. Summary and conclusions

Light scattering by assemblies of cloud particles can generate depolarization of the incident energy through two scattering processes. The first, which may be regarded as a source of noise in some remote sensing applications, is the multiple-scattering process in which the depolarization is generated by virtue of inter-particle scattering involving two or more cloud particles, the last of which resides in the detector's field of view. The second process, which provides the foundation for the discrimination of cloud particle thermodynamic phase, involves the rotation of the incident vibration plane through internal reflection within a single element. Our polarization measurements demonstrate that the dominant depolarizing process is a function of cloud particle shape. Whereas

depolarization in water clouds is a function of cloud optical thickness, an indication of the amount of multiple-scattering activity present, ice cloud depolarization is appreciably more intense and less sensitive to cloud optical thickness.

Angular depolarization patterns from water clouds show that the generation of multiple-scattering-induced depolarization is basically a backscattering phenomenon, as has also been inferred from the behavior of lidar pulses in cumulus clouds (Houston and Carswell, 1978). Only small amounts of depolarization on the order of our experimental uncertainties have been measured in the forward scattering direction, but the δ values then increase significantly with increasing scattering angle. However, irregularities in the δ value patterns appear to indicate that the generation of the depolarized component is not a simple function of the scattering angle. In addition, differences in the generation of depolarization with the incident polarization direction are indicated to be proportional to the degree of linear polarization. Thus, it seems that the magnitude of the depolarized component may be independent of the incident polarization state. In approaching true backscattering, both the scattered intensities and δ values increase strongly so that the impact of the depolarized component becomes significant. Measurements performed at $\theta=175°$, the closest angle to the backscatter as permitted with the present system design, reveal a linear dependence of δ with cloud optical thickness through the range of about $0.15<\tau'<0.9$. Thus, a linear increase in δ with lidar pulse penetration depth into some regions of relatively homogeneous water clouds may be expected, an occurrence often noted in lidar studies (see, e.g., Houston and Carswell, 1978).

Clouds composed entirely of ice crystals exhibit a similar trend of increasing δ values with increasing scattering angle, in accordance with the belief that the contributions from multiple internal reflections should become significant in scanning away from the forward-scatter diffraction regime. Scattered energy contributions from specular reflections are apparently not very significant, as evidenced by the fact that values of δ_V and δ_H fail to display the dependence to be expected from the variations in Fresnel reflection coefficients with scattering angle and incident polarization direction. If this were to be the case, δ_H values would be considerably higher in the side scatter, particularly in the vicinity of the Brewster angle of $\theta\approx80°$ with reference to the nephelometer scattering geometry. However, measurements show that depolarization ratios for either incident polarization direction are usually rather similar in the region of rapidly increasing δ values for $\theta\lesssim140°$. In approaching the backscatter, δ_V and δ_H values display dissimilar patterns, although it can be assumed that the δ values increase to ~0.50 regardless of the incident polarization direction due to the presence of axial symmetry at $\theta=180°$ (Sassen, 1974).

Concerning the influence of ice cloud composition on depolarization, we have noted a tendency for particularly the δ_V values to increase somewhat in the side-scatter region with increasing crystal thickness or size over the limited size range of particles generated in our chamber. The impact of ice cloud optical thickness on depolarization appears also to cause an increase in side-scattering intensity and depolarization when very dense ice clouds are examined. On the other hand, measurements performed at $\theta=175°$ have not indicated significant multiple-scattering-induced depolarization increases in the backscattering region. This can also be inferred from most lidar measurement of ice clouds (see, e.g., Sassen, 1976, 1978b; Pal and Carswell, 1977).

In accordance with the differences in ice and water cloud angular scattering efficiencies discussed in Part I, depolarization in clouds of mixed-phase composition displays a dependence on cloud ice-water balance which would appear to hold significant potential for the inference of cloud composition through bistatic remote sensing techniques. Mixed-phase clouds containing relatively small amounts of water droplets can be identified through polarization measurements performed in the cloudbow region where δ value troughs are produced as a result of the strong and highly linearly polarized scattering contributions from the spherical particles. Conversely, due to the greater side-scattering efficiency of ice crystals, small amounts of ice in a water cloud can be identified by depolarization measurements in the side-scattering region. Thus, it appears that the great differences in water-ice particle scattering efficiency, as illustrated in Part I, and depolarization in the cloudbow and side-scattering regions can be utilized in the design of bistatic remote sensing experiments for the assessment of cloud ice-water balance. In the backscattering region, estimates of the backscatter-to-extinction ratios for water and ice clouds reveal that atmospheric cloud droplet assemblies are on the order of 5–10 times more efficient at backscattering than clouds of similarly sized ice crystals. These various effects combine to produce a characteristic angular depolarization pattern for clouds containing significant amounts of both water and ice particles which displays a peak in the side-scatter region.

In addition to contributing to our basic understanding of the scattering behavior of nonspherical particles and the multiple-scattering process, the angular depolarizing experiments described here clearly have application in the fields of passive and active remote sensing of clouds and planetary atmospheres. Bistatic remote sensing observations performed at scattering angles where differences in water-ice particle scattering behavior are most pronounced appear to be particularly promising for the inference of mixed-

phase cloud composition. For future studies to further evaluate the information content of scattered laser signals and improve our physical understanding of the scattering by nonspherical particles, similar laboratory investigations should be performed in a manner which would allow the polarization characteristics of the scattered light to be completely parameterized for various incident polarization states, with special attention given to the backscattering region.

Acknowledgments. This research was supported by the Atmospheric Research Section of the National Science Foundation under Grant ATM 75-05216. We would like to thank S. P. Hunder and P. Flatt for their contributions to the experimental program.

REFERENCES

Holland, A. C., and G. Gagne, 1970: The scattering of polarized light by polydisperse systems of irregular particles. *Appl. Opt.*, **9**, 1113–1121.

Houston, J. D., and A. I. Carswell, 1978: Four-component polarization measurements of lidar atmospheric scattering. *Appl. Opt.*, **17**, 614–620.

Liou, K. N., 1972: On depolarization of visible light from water clouds for monostatic lidar. *J. Atmos. Sci.*, **29**, 1000–1003.

——, and R. M. Schotland, 1971: Multiple backscattering and depolarization from water clouds for a pulsed lidar system. *J. Atmos. Sci.*, **28**, 772–784.

Pal, S. R., and A. I. Carswell, 1973: Polarization properties of lidar backscattering from clouds. *Appl. Opt.*, **12**, 1530–1535.

——, and ——, 1977: The polarization characteristics of lidar scattering from snow and ice crystals in the atmosphere. *J. Appl. Meteor.*, **16**, 70–80.

Platt, C. M. R., and K. Bartusek, 1974: Structure and optical properties of some middle-level clouds. *J. Atmos. Sci.*, **31**, 1079–1088.

Sassen, K., 1974: Depolarization of laser light backscattered by artificial clouds. *J. Appl. Meteor.*, **13**, 923–933.

——, 1976: Polarization diversity lidar returns from virga and precipitation: Anomalies and the bright band analogy. *J. Appl. Meteor.*, **15**, 292–300.

——, 1978a: Backscattering cross sections for hydrometeors: Measurements at 6328 Å. *Appl. Opt.*, **17**, 804–806.

——, 1978b: Air-truth lidar polarization studies of orographic clouds. *J. Appl. Meteor.*, **17**, 73–91.

——, and K. N. Liou, 1979: Scattering of polarized laser light by water droplet, mixed phase, and ice crystal clouds: Part I. Angular scattering patterns. *J. Atmos. Sci.*, **36**, 838–851.